Available online at http://docs.lib.purdue.edu/jate

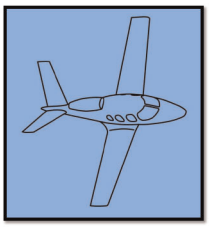

JATE

Journal of Aviation Technology and Engineering 12:2 (2023) 35–52

Comparative Evaluation of Investigation Methods for Estimating the Load-Dependent State of Charge and End of Discharge of a Multirotor UAV Battery

Hanna Dibbern[1], Morten Roßberg[1], and Claudia Werner[1]

[1]*Flensburg University of Applied Sciences*

Abstract

As the scope of multirotor unmanned aerial vehicle (UAV) applications increases, more attention is being paid to UAV energy requirements, which vary depending on the mission profile. To obtain accurate information about the UAV battery during flight, the idea of a digital twin including a battery state estimation model is promising. For battery state estimation, a Kalman filter combination is the preferred approach in the literature. Comparing different Kalman filters, the unscented Kalman filter has a more accurate estimation for nonlinear systems compared to the extended Kalman filter. In the application of UAV flight with load-dependent flight missions, the comparison of different Kalman filter estimation methods has not yet been researched. In order to evaluate the applicability of different state of charge estimation methods applied to different UAV flight missions, an extended Kalman filter, an unscented Kalman filter, and the Coulomb-counting method are implemented in this research and combined with an end of discharge estimation. To compare the estimation methods based on a delivery mission and a facade inspection mission, a parameter identification of the UAV battery is performed, and an equivalent circuit model is developed and combined with the estimation methods to estimate the battery state. The results of the investigation show that the unscented Kalman filter achieves more accurate state of charge estimation results than the extended Kalman filter, even in the field of UAV application. The results also show that the choice of estimation method is mainly influenced by the accuracy of the parameter identification process, while the dynamic load of a UAV mission has less impact. Contrarily, the end of discharge estimation does not correlate with the accuracy of the state of charge estimation, indicating that the end of discharge estimation is more dependent on the dynamic load.

Keywords: multirotor UAV, battery modeling, state of charge, end of discharge, Kalman filter, Coulomb-counting

1 Introduction

Multirotor electrically powered unmanned aerial vehicles (UAVs) have been studied and deployed in various application areas such as monitoring (Possoch et al., 2016), delivery (Ayamga et al., 2021), and drone show (Lanteigne et al., 2017).

For the operator of a UAV, it is of interest to know the state of the battery in order to evaluate the progress of a flight mission and its limits. During a mission, the UAV is exposed to fluctuating power requirements due to mission

https://doi.org/10.7771/2159-6670.1293

characteristics and environmental conditions, which can lead to varying battery power requirements. Usually, a battery management system is used to monitor and limit the operation of the battery in order to protect it from health degradation (Naseri et al., 2023).

However, with the advancement of new technologies, digital twins have been discussed in various applications such as general model-based systems (Madni et al., 2019), agriculture (Nasirahmadi & Hensel, 2022), healthcare (Boulos & Zhang, 2021; Hassani et al., 2022), UAV and internet of things-based systems (Sun et al., 2022), and batteries (Singh et al., 2021; Thelen et al., 2022). In UAV applications, a digital twin can be used to limit operational risks and gain new insights into the processes and condition of the UAV (Fakhraian et al., 2023), as well as to minimize time and energy requirements through optimized path planning (Soliman et al., 2023).

A basic exemplary model on the way of developing a full digital twin of the UAV battery application could use the real-time voltage and current data from the real battery and process the information to estimate the remaining capacity and state of charge (SOC), and to predict the end of discharge (EOD). This information could be presented to the UAV pilot who could take early action to limit the mission to a safer operating range to extend the battery health.

For the future development of a digital twin, a reliable battery model is necessary. Several battery modeling approaches have been developed and discussed in the literature (Meng et al., 2018; Shrivastava et al., 2019). Recently, there has been an increase in research on artificial intelligence data-driven and machine learning methods especially for SOC and state-of-health estimations in aerial applications (Raoofi & Yildiz, 2023; Shibl et al., 2023) as well as in electromotive applications (Khawaja et al., 2023; Manoharan et al., 2023).

Nevertheless, for real-time estimation, an electrical equivalent circuit model combined with a variation of a Kalman filter is also commonly used due to its accurate SOC estimation (Khanum et al., 2021; Sangwan et al., 2017). The most popular variations of the Kalman filter for SOC estimation in general are the extended Kalman filter and the unscented Kalman filter. For nonlinear systems, the unscented Kalman filter is superior to the extended Kalman filter due to robustness and higher accuracy as illustrated by several comparative studies (Guo et al., 2023; He et al., 2013; Kumar & Rao, 2023; Priya et al., 2022).

Regarding UAV applications, Schacht-Rodriguez et al. (2017) presented a model with an extended Kalman filter for SOC and EOD estimation and applied it in a flight mission. In addition, Anggraeni et al. (2022), Jung & Jeong (2017), and Zhang et al. (2019) presented SOC estimation methods using the extended Kalman filter and managed to achieve low SOC estimation errors. As the focus of research regarding UAV applications has not yet been on the unscented Kalman filter utilization for SOC estimation and general research shows advantages compared to the extended Kalman filter, this paper considers both estimation methods and the basic Coulomb-counting method to comparatively evaluate the best estimation performance while conducting different UAV flight missions.

The objective of this paper is to comparatively evaluate an equivalent circuit battery model in combination with different Kalman filters and the Coulomb-counting method to find the most appropriate estimation method for the load-dependent SOC and EOD of a multirotor UAV battery. The results of this paper will be used to determine which Kalman filter estimation method is most applicable to UAVs for the further development of digital twins of UAV batteries in the future.

This paper first introduces the UAV under study, its battery parameters, and the two investigated flight missions in Section 2. This is followed by the battery modeling process, including the parameter identification and the SOC and EOD estimation methods. In Section 3, the simulation results of the flight mission are presented, and in Section 4, the conclusion of this paper and an outlook are given.

2 UAV Battery Estimation Modeling Process

For the following comparative evaluation of the different SOC and EOD estimation algorithms in the UAV application area, the basic correlations outlined in Figure 1 were considered.

The individual steps of the components are described in the following. During an ongoing flight mission, the UAV battery (see Section 2.1) has to provide the required power (see Section 2.2). The time-varying load requirements, current, and voltage are measured by sensors and provided as input signals to the developed battery state estimation model. The model uses an electrical equivalent circuit battery model (see Section 2.3), which provides the calculated voltage to the Kalman filter (see Section 2.5). The measured current also serves as an input signal to the Kalman filter (extended Kalman filter (see Section 2.5.1) or unscented Kalman filter (see Section 2.5.2)). The estimated SOC of the Kalman filter is used to estimate the EOD (see Section 2.5.3). The SOC and EOD are presented in real time to the UAV pilot, who can monitor the estimates and take countermeasures such as reducing power or returning early if the planned mission and the estimated EOD do not match. A more detailed description of the battery model and the developed state estimation model is given in the following subsections.

2.1 Description of the UAV

The investigated lithium battery-powered multirotor UAV is based on an exemplary commercial UAV (Matrice 600 Pro—DJI, n.d.). It is a multirotor UAV with six rotors and a weight of 10 kg, which can carry an

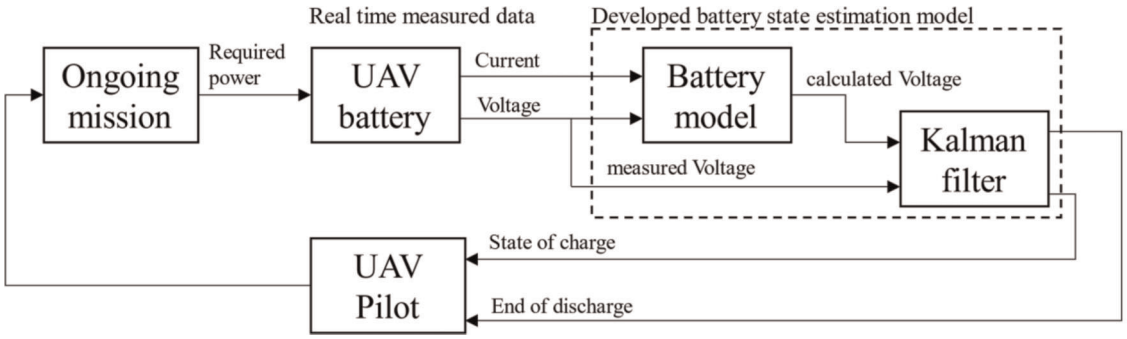

Figure 1. Basic overview of the interrelationships between the developed battery state estimation model and the UAV battery.

additional payload of up to 5.5 kg, depending on the mission. The UAV is equipped with six batteries to store a maximum energy of 779.76 Wh (Matrice 600 Pro—DJI, n.d.).

In this first approach to the battery model, MATLAB and Simulink components are used as the output signal of the investigated battery. The assumed battery is modeled using the Simscape Electrical Battery (Table-Based) block. Here, predefined data points or series can be added to various parameters, including capacity, open-circuit voltage, terminal resistance, and several different modeling options, all as a function of the SOC. These parameters were taken from one of the internal example Simulink models provided by Mathworks itself (Huria et al., 2012; Lithium Battery Cell—Mathworks, n.d.).

Since the cell capacity and nominal voltage of the UAV battery (reference UAV) and the model battery are different, the number of cells per battery and batteries per UAV were adjusted for the model to achieve similar values of stored energy. The general parameters are listed in Table 1.

Table 1
Comparison of reference UAV battery parameters (Matrice 600 Pro—DJI, n.d.) and battery parameters of the used battery model (Lithium Battery Cell—Mathworks, n.d.).

	Reference UAV battery	Battery model
Cells per battery	6	7
Batteries per UAV	6	8
Cell capacity	5.70 Ah	4.18 Ah
UAV capacity	34.20 Ah	33.40 Ah
Nominal cell voltage	3.80 V	3.30 V
Nominal UAV voltage	22.80 V	23.10 V
Stored energy	779.76 Wh	771.54 Wh

2.2 Description of Flight Missions

The model is intended to work with real-time data from a UAV on an ongoing mission. In the first approach this research uses MATLAB and Simulink components and multirotor UAV power profiles from different flight missions as input to the model. Figure 2 shows how the power profiles are integrated into the model described at the beginning of Section 2.

Two different missions, a delivery flight mission and a monitoring mission described by Suwe et al. (2022), are investigated. In the delivery mission, the UAV picks up a package weighing 2 kg from point A, delivers it to point B, and then returns to point A without the package on the same path. The flight path is shown in Figure 3.

In detail, the UAV goes from no motion to an accelerated climb to gain vertical speed, followed by a constant climb to the desired altitude of 120 m. After reaching the altitude above point A, the UAV hovers for 10 s and transitions to an accelerated horizontal flight to a constant horizontal flight at a speed of 12 m/s for 5 km until point B is reached. Upon arrival, the UAV hovers above the point again for 10 seconds, then descends and lands. After delivering the package, the UAV returns while performing the above actions in reverse without the package attached. The total horizontal flight distance is 10 km, and the total flight time is 1006.2 s. The resulting power profile calculated by Suwe et al. (2022) and shown in Figure 4 is used as input to the model.

For the facade inspection mission, a monitoring flight in the form of a facade inspection flight mission was described by Suwe et al. (2022). Monitoring missions have been used to inspect buildings, bridges, and power lines to detect possible damage to the structure. In this study case a five-story building with a height of 15 m and a length and width of 50 m is assumed to be inspected stock-wise horizontally. The UAV is equipped with camera equipment weighing 1.6 kg. The flight path is shown in Figure 5.

From the starting point in one of the corners of the building, the UAV accelerates vertically, climbs constantly to 1.5 m, and hovers at this position for 5 s. After the hover, the UAV transitions to an accelerated horizontal flight, followed by a constant horizontal flight at a speed of 2 km/h, and travels around the building at a distance of 3.5 m from the building. After completing the inspection of the first floor, the UAV hovers above the start point for 5 s, climbs 3 m to the second floor, and hovers again for 5 s. The UAV transitions back to an accelerated horizontal flight and repeats the inspection for each subsequent floor until the fifth floor is completed, at which point the UAV returns to the ground. The duration of the entire mission is 619 s.

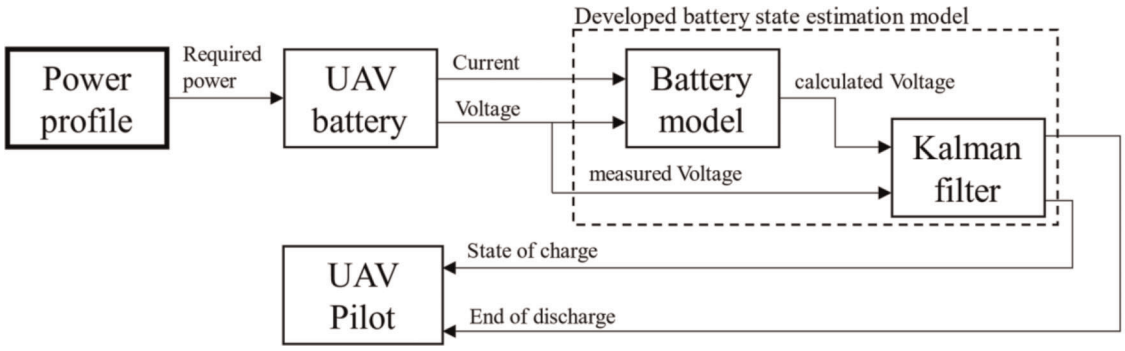

Figure 2. Integration of the power profiles into the assumed interrelationships of the developed battery state estimation model and UAV battery.

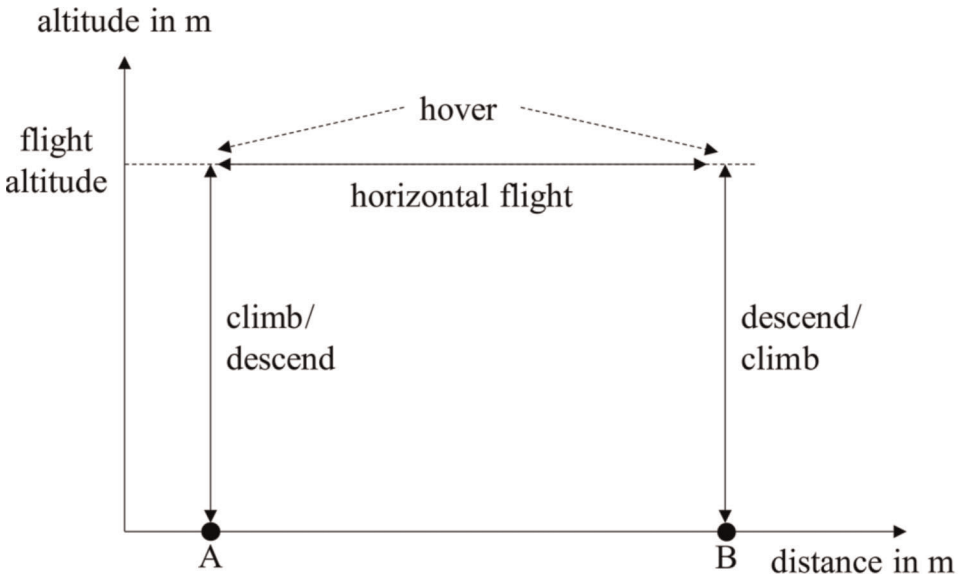

Figure 3. Basic outline of the delivery flight mission (Suwe et al., 2022).

The resulting power profile calculated by Suwe et al. (2022) and shown in Figure 6 for the facade inspection is used as input to the model.

The discussed load profiles apply to the following assumptions and constraints. External environmental conditions such as wind speed and direction have not been included. The ambient temperature and the battery temperature have been assumed to be constant, independent of the altitude. The ambient pressure as well as precipitation and humidity are not considered. Furthermore, the user behavior has not been taken into account. For the following investigations of the estimation methods, these load profiles are used in order to have a consistent basis for comparison in the first step. For further investigations of real UAV applications, it should be considered that a variation of the environmental conditions and user behavior will affect the energy demand of the UAV.

2.3 Description of the Battery Model

The purpose of the battery model to be studied is to replicate the behavior of the real battery as closely as possible. In this paper, a dual polarization electrical equivalent circuit model (2RC or second order) is used to represent the battery, as it has been shown to better represent a real battery compared to the first-order model, while remaining less complex than higher-order models (Huria et al., 2013). It uses two RC networks to describe the transient dynamics, as shown in Figure 7. R_i represents the ohmic resistance and R_1, C_1, R_2, and C_2 represent the internal polarization resistance and capacitance of the battery. V_1 (R_1, C_1) and V_2 (R_2, C_2) are the voltage drops across the respective RC networks. These parameters depend on SOC and have to be identified. The open-circuit voltage V_0 is represented as a voltage source that also varies ($V_0 = f\,(\mathrm{SOC})$). Using Kirchhoff's second law, the voltage equation can be written as:

$$V_{bat}(\mathrm{SOC}) = V_0(\mathrm{SOC}) - R_i(\mathrm{SOC}) \cdot I_{bat} - V_1(\mathrm{SOC}) - V_2(\mathrm{SOC}) \qquad \text{(Eq. 2.1)}$$

The primary purpose of this battery model is to evaluate the effects on SOC estimation and EOD estimation. Therefore, no additional dependencies, such as the influence of

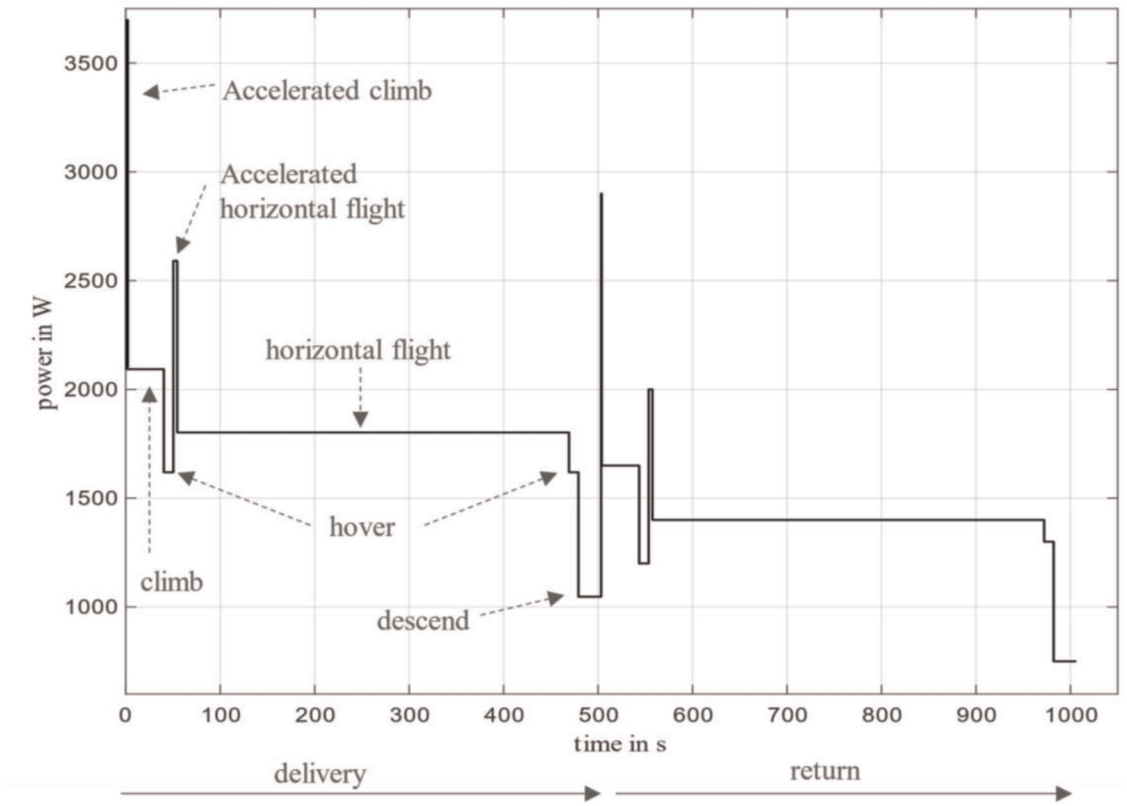

Figure 4. Power profile of the delivery mission from Suwe et al. (2022).

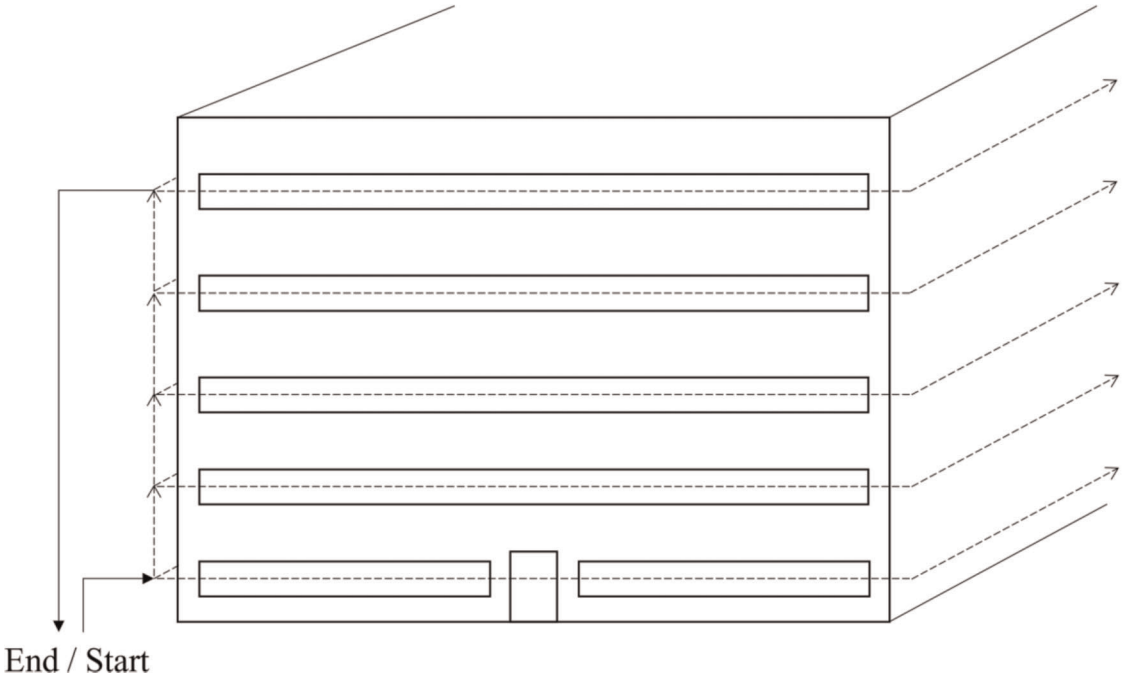

Figure 5. Basic outline of the facade inspection mission (Suwe et al., 2022).

ambient temperature discussed in Hu et al. (2023), the thermal modeling of the battery presented in Zhu et al. (2013), or the influence of degradation mechanisms according to Krupp et al. (2022) and Zhao et al. (2017), are considered. This model assumes a constant temperature of 16.6℃, which corresponds to the average temperature in New York City (Klima New York City, n.d.). However, for future studies, a combination of different loads and

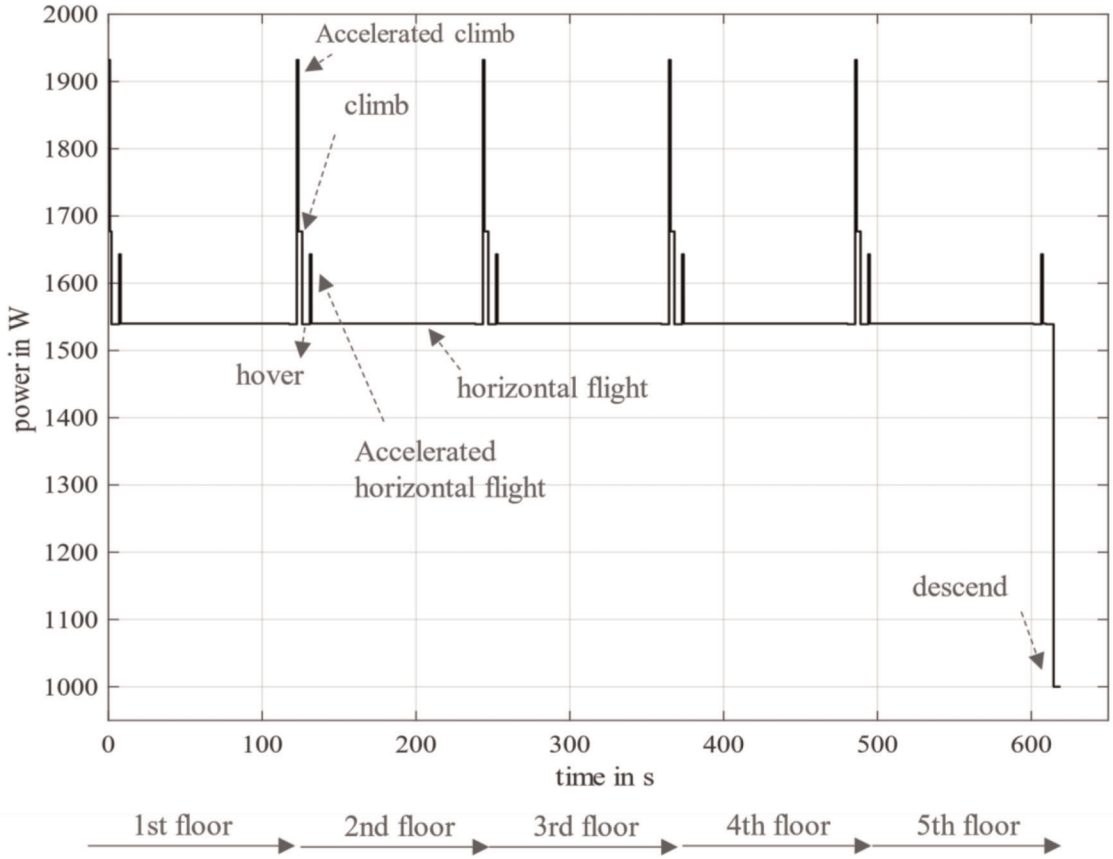

Figure 6. Power profile of the facade inspection mission from Suwe et al. (2022).

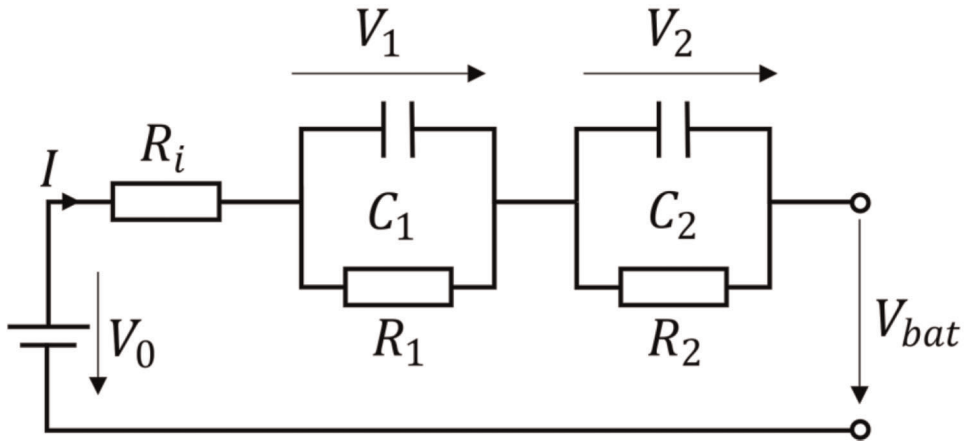

Figure 7. Equivalent circuit diagram of the 2RC battery model during discharge.

temperatures as well as thermal modeling of the battery according to the approach presented in Zhu et al. (2013) should be considered. In addition, the implementation of degradation effects to estimate the state of health as described in Liu et al. (2022) is strongly recommended.

2.4 Parameter Identification of the Battery

The battery model depends on the different equivalent circuit components shown in Figure 7. The components must be identified to make an accurate representation of the battery possible. In this identification process, the battery must go through tests, starting with a simple capacity test to find the true capacity. To do this, the battery is charged and then completely discharged, monitoring the current and time required to completely discharge the battery.

For the equivalent circuit representation of the battery, the parameters R_i, R_1, C_1, R_2, and C_2 must be identified in another process. To identify the parameters, the widely used analysis method presented by Lv et al. (2020) and

Santos et al. (2017) is used. For each SOC step, the response of the voltage to a constant current pulse must be examined. An example response is shown in Figure 8.

Sections A–B and C–D show the instantaneous response to the applied current pulse. This drop and rise in voltage during discharging is due to the internal ohmic resistance of the battery, $R_i \cdot R_i$ can be found directly from the four voltages corresponding to points A–D and the discharge current I_{bat} for each SOC step:

$$R_i(\mathrm{SOC}) = \frac{(V_B - V_A) + (V_C - V_D)}{2 \cdot I_{bat}} \qquad \text{(Eq. 2.2)}$$

The two RC networks are used to describe the exponential response in sections B–C and D–E. The time constants τ_1 and τ_2 (where $\tau_1 = R_1 \cdot C_1$; $\tau_2 = R_2 \cdot C_2$) are used to describe the dynamic behavior. The identification of R_1 and R_2 and the time constants τ_1 and τ_2 needs to be approached through optimization using the MATLAB Toolbox Curve Fitter and a least-squares fitting function on the named exponential responses.

The final step in the identification process is to characterize the open-circuit voltage V_0. This is done by noting the resulting voltage after the relaxation phase of the current pulse (point C in Figure 8) for each SOC step examined.

The results of the parameter identification are shown in Figure 9. As can be seen in Figure 9A, the open-circuit voltage V_0 follows the typical battery voltage characteristics with an exponential zone between 90% and 100%, a wide nominal zone with only a small change in voltage representing the main operating range, and a stronger voltage decrease at 20% and below when the nominal zone ends.

The corresponding parameters for the resistors shown in Figure 9B are on the same scale to show the different magnitudes of the parameters. The parameters R_i, R_1, and R_2 are relatively constant and vary only slightly in the range from 20% to 80% SOC which is the main operating range. Outside the operation range, in the range of 0% to 20% and 80% to 100% especially the resistance R_2 increases. Considering this operating range, this paper takes the average values as the battery parameters to be used in the following SOC estimation process to reduce the nonlinearity of the system. The results of the identification process are shown in Table 2.

2.5 Estimating the SOC and the EOD

As shown in Figure 10, different methods can be used to determine the SOC of the battery, which are described in Zhou et al. (2021) and Boulmrharj et al. (2020). The estimation methods can be divided into three main groups.

From the group of direct methods, only the Coulomb-counting method is considered as the SOC estimation method in this paper because it is simple and one of the most widely used methods (Saji et al., 2019). The Coulomb-counting method uses the measured current I_{bat} integrated over time to estimate the SOC with the help of the SOC value in the step before SOC_0, nominal capacity C_n, and the battery efficiency η (Boulmrharj et al., 2020):

$$\mathrm{SOC} = \mathrm{SOC}_0 - \frac{\eta}{C_n} \cdot \int_{t-1}^{t} I_{bat} \cdot dt \qquad \text{(Eq. 2.3)}$$

The second group of estimation methods are the artificial networks that have high accuracy. All methods in this group require reliable training data to achieve good performance (Zhou et al., 2021). Since no reliable training data are known for the UAV under study, these methods are not considered.

The third group consists of the model-based methods, which can be divided into observer, Kalman filter, and particle filter. These methods use the model and the measurement to estimate and correct the state of the model. Observers such as the adaptive Luenberger observer can be used to estimate the SOC as in Hu et al. (2010). The Kalman filter is only suitable for linear systems, while the

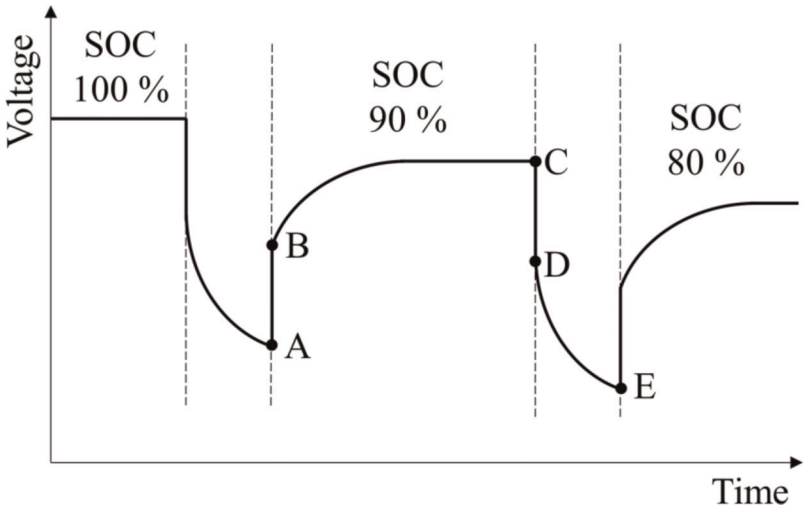

Figure 8. Voltage response to a constant current pulse based on Jackey et al. (2013).

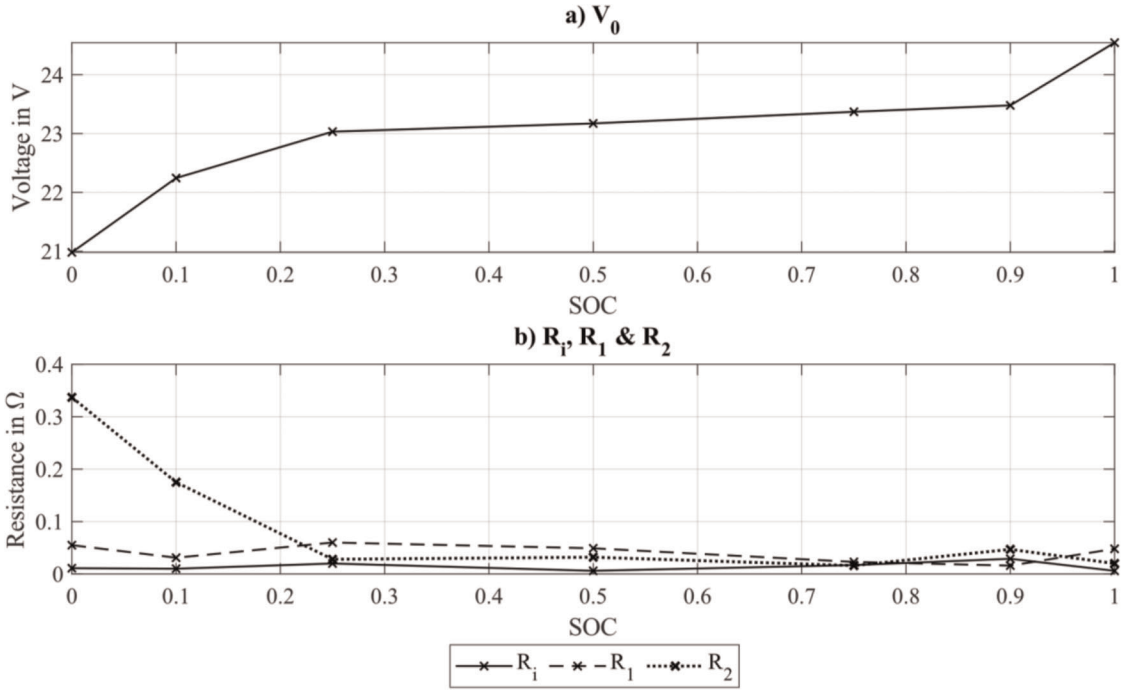

Figure 9. Identified parameter values of the battery. (A) Open-circuit voltage. (B) Internal resistance and the two polarization resistances.

Table 2
Result of battery parameter identification.

R_1	R_2	τ_1	τ_2
0.044 Ω	0.0253 Ω	668 s	270 s

unscented Kalman filter, extended Kalman filter, and their adaptive counterparts are suitable for nonlinear systems. Since the chosen model depends on the SOC, it is a nonlinear system. Detailed descriptions of the Kalman filter types and their advantages and disadvantages are presented in Zhou et al. (2021). In addition, particle filters can be implemented for highly nonlinear systems as in Ye et al. (2018).

Combinations of the methods can also be used to reduce the estimation error. Possible hybrid methods are described in Boulmrharj et al. (2020). One of the hybrid methods presented in that paper is the combination of the Kalman filter with Coulomb-counting (Boulmrharj et al., 2020).

Consequently, this paper implements the SOC estimation with Coulomb-counting in combination with a nonlinear extended and unscented Kalman filter. The Coulomb-counting estimation is also evaluated.

2.5.1 Development of the extended Kalman filter

To develop an extended Kalman filter, the model needs to be transformed into a state space model. The discrete state space model is derived as described in Shrivastava et al. (2019) and Sepasi et al. (2014). A simplified overview of the algorithm is shown in Figure 11A.

First the Jacobian of the measurement matrix (H) is computed, which is a matrix of all first-order partial derivatives. In the prediction step, the state variables (V_1, V_2, and SOC) and the covariance matrix (P) are updated. The correction step corrects the state variables and the covariance matrix with respect to the deviation of the calculated V_{bat} and the measured voltages (V_{meas}). The algorithm of the extended Kalman filter is explained in detail inSchacht-Rodriguez et al. (2017).

In contrast to the work of Schacht-Rodriguez et al. (2017), a dependence between R_i and the SOC is assumed as in He et al. (2013). Thus, the Jacobian of the measurement matrix ($\underline{H}$) for a 2RC model is computed as a partial derivative with respect to all state variables:

$$\underline{H} = \begin{bmatrix} -1 & -1 & \dfrac{\delta V_0}{\delta \text{SOC}} - I_{bat} \cdot \dfrac{\delta R_i}{\delta \text{SOC}} \end{bmatrix} \qquad \text{(Eq. 2.4)}$$

To find the derivative of the open-circuit voltage with respect to the SOC δV_0 / δSOC and the derivative of the internal resistance with respect to the SOC δR_i / δSOC, the dependencies can be approximated with a linear polynomial function as in He et al. (2013). Another approach is to construct the difference quotient and linearize the function around the operating point. Both approaches lead to similar solutions for this type of battery.

2.5.2 Development of the unscented Kalman filter

To improve results and to be more robust to nonlinear systems, an unscented Kalman filter is also implemented and tested. A brief overview of the unscented Kalman filter is given in Figure 11B. Overall, the unscented Kalman filter does not use the Jacobian to estimate the actual state but uses sigma points from the Gaussian distribution to

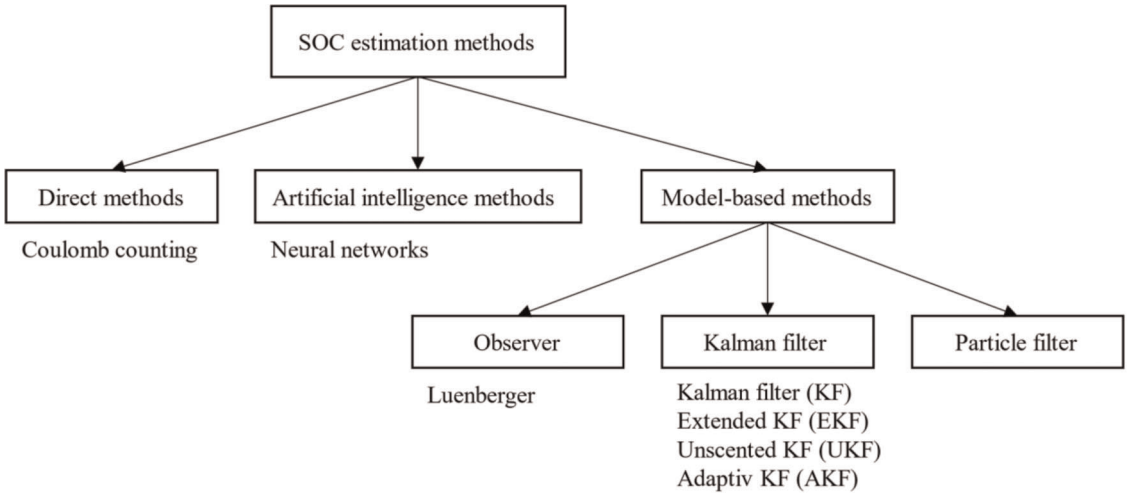

Figure 10. Overview of relevant SOC estimation methods for this paper from Boulmrhaj et al. (2020).

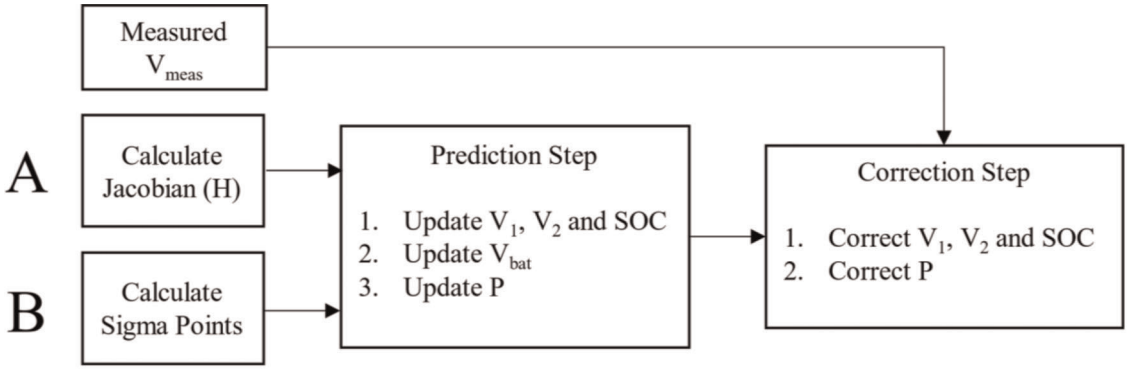

Figure 11. Overview of the different Kalman filter-based estimation algorithms. (A) Extended Kalman filter. (B) Unscented Kalman filter.

estimate the actual state. In the prediction step, the new states are calculated using the sigma points and the resulting battery voltage (V_{bat}) is calculated. Additionally, the covariances (P) are determined. In the correction step, the states are corrected as well as the covariance (Lv et al., 2020; Zhang et al., 2022). A detailed explanation as well as the algorithm can be found in He et al. (2013).

To compare both Kalman filters and the Coulomb-counting method the root-mean-square error (RMSE) is calculated (Huang et al., 2018). The RMSE is the quadratic difference between the real value (x) and the estimated value ($\hat{x}$) divided by the number of sample points (n):

$$\mathrm{RMSE} = \sqrt{\frac{1}{n} \cdot \sum_{t=1}^{n} (\hat{x} - x)^2} \qquad \text{(Eq. 2.5)}$$

Additionally, the maximum deviation between the actual and the estimated SOC is determined by subtracting the actual values from the estimated values:

$$MAX = \max | \hat{x} - x | \qquad \text{(Eq. 2.6)}$$

2.5.3 EOD estimation

A linear approximation is used to estimate the EOD from the estimated SOC. The actual SOC(t) is calculated from the initial SOC_0 and its derivation (Schacht-Rodriguez et al., 2017):

$$\mathrm{SOC}(t) = \Delta\mathrm{SOC} \cdot t + \mathrm{SOC}_{t-1} \qquad \text{(Eq. 2.7)}$$

This equation calculates the EOD and uses the exponential moving average to smooth the result. Depending on the variability of the SOC estimate, the smoothing can be adapted.

3 Results and Discussion

To analyze the behavior of the UAV battery in terms of the SOC and EOD estimation, the two missions presented are simulated. Before presenting the results, the general conditions of the simulation are described.

The investigated battery has an initial SOC of 95%, which covers possible self-discharge reactions inside the battery, while the estimation methods have an initial SOC of 100%. This difference is intentional, as the estimation methods need to react accordingly to a deviation from the

real battery and need to be able to estimate the SOC with varying initial conditions.

The EOD estimation uses the lower end of the described working range of the battery (at 20% SOC) as the EOD reference point.

3.1 SOC Estimation for Flight Missions

Figure 12 shows the corresponding voltage and current profiles of the battery in response to the power profile of the delivery flight mission. Initially, the highest power is required during the accelerated climb, so a high current is present. During horizontal flight, the interaction between voltage and current is evident. As the battery voltage drops because of the decreasing SOC, the current increases to compensate and still deliver the required power. Overall, the battery voltage drops from about 22 V to a voltage of about 16 V. The average current of the mission is 86.61 A.

The actual and estimated SOCs are shown in Figure 13. The estimated SOCs at the end of the mission are compared in Table 3. At the end of the mission, the SOC remains at approximately 22%. This is only 2% above the lower end of the main operating range. Thus, the mission can just be completed by the battery. Both estimation methods with Kalman filters adjust their estimation to the real SOC value and are able to track the change in SOC. The deviation at the end of the mission is only 0.62% for the unscented Kalman filter and 2.52% for the extended Kalman filter. The deviation of the Coulomb-counting method at the end of the mission is the highest with 5.2%.

Figure 14 shows the SOC deviation during the mission. The estimation of the Coulomb-counting method does not adapt to the real SOC because it has no way to correct its state variables when they differ from the initial SOC. Thus, the offset of 5% of the initial condition remains until the end of the mission. For the Kalman filters, the highest deviation is at the beginning of the simulation due to the different initial condition of the SOC. Interestingly, both Kalman filters respond quickly to the SOC deviation, but the extended Kalman filter is not able to eliminate the error completely. Due to the nonlinearity, the unscented Kalman filter achieves better results as expected and described in He et al. (2013). The unscented Kalman filter is able to eliminate the estimation error extremely quickly while also staying close to the real SOC value.

It can also be seen that the deviations of the filters depend on the accuracy of the parameters. As the parameters are only identified for discrete points, the deviation also depends on the parameter identification.

Table 4 shows the maximum deviation and the RMSE of the estimation methods. The maximum deviation of the extended and the unscented Kalman filters, as well as the maximum deviation of the Coulomb-counting method are high compared to the RMSE. This is due to the different initial conditions at the beginning of the simulation. However, the extended Kalman filter and the unscented Kalman filter perform significantly better than the Coulomb-counting method. Comparing the two Kalman filters, the RMSE of the unscented Kalman filter is about 1.45% smaller than the RMSE of the extended Kalman filter.

The second simulated mission is the facade inspection mission. Since this is a shorter mission compared to the delivery flight mission, higher SOC values are expected at the end of mission. Figure 15 shows the voltage and current response to the mission power profile. It can be seen that

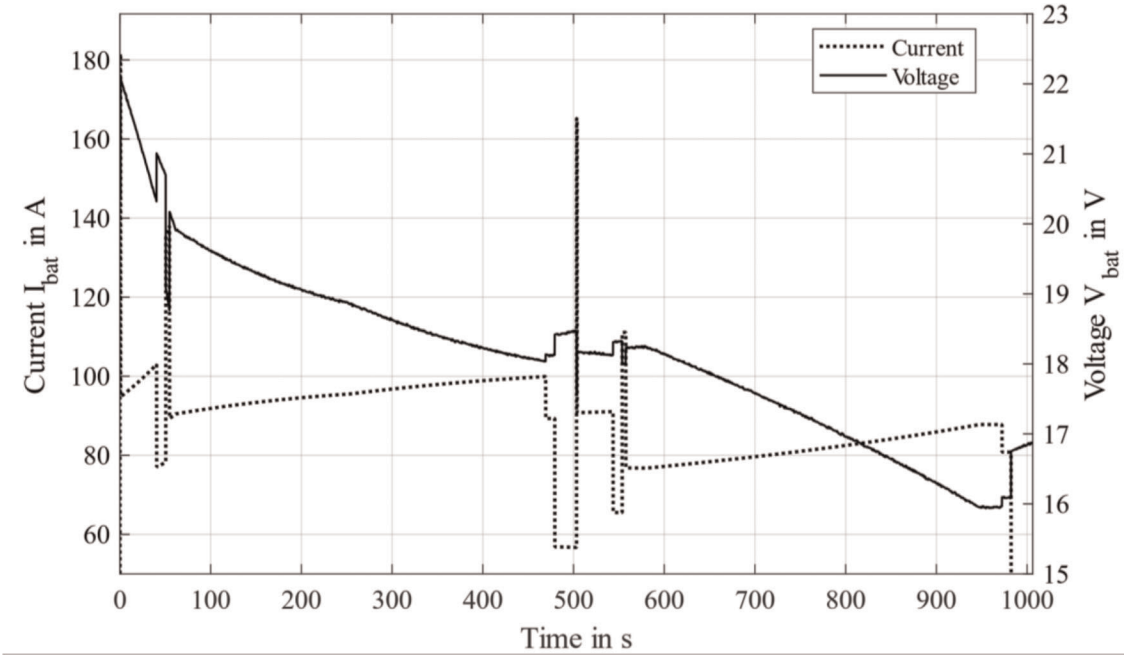

Figure 12. Resulting voltage and current profiles of the UAV battery during the delivery flight mission.

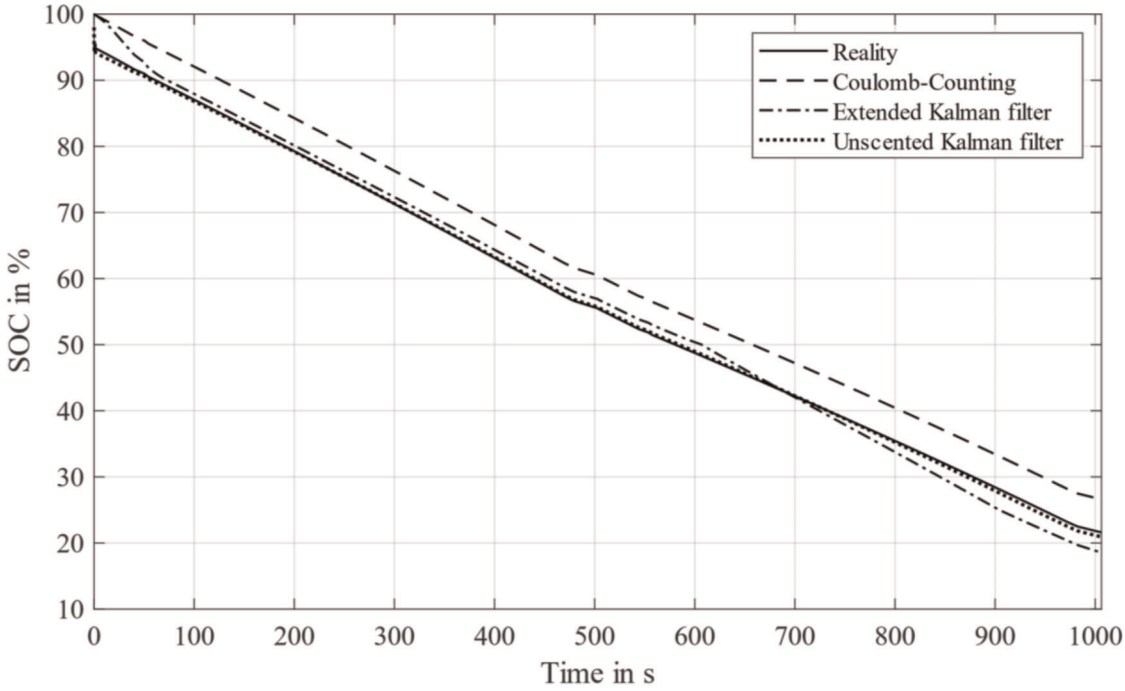

Figure 13. Resulting SOC profiles of the UAV battery and the estimation methods during the delivery flight mission.

Table 3
Comparison of the end of mission SOC values of the battery and the respective estimation method for the delivery mission.

Battery	Unscented Kalman filter	Extended Kalman filter	Coulomb-counting
21.59%	20.97%	19.07%	26.79%

the voltage and current interact as expected as the current compensates for the voltage drops and reverses to deliver the required power. The voltage drops from about 22.5 V to 18.5 V during the mission. The average current is 79.24 A.

The SOC at the end of the mission, shown in Figure 16 and Table 5, ends with about 54% of the remaining energy. The discharge rate of the facade inspection mission is about 9% less than the discharge rate of the delivery mission. The reason for this can be explained with the help of the average current. The average current is 79.24 A which is about 8.51% less than the average current of the delivery mission. The estimated and the real SOCs at the end of the façade inspection mission are depicted in Table 5. The deviation at the end from the unscented Kalman filter is 0.23% and the deviation from the extended Kalman filter is 1.73%. The Coulomb-counting method has the biggest deviation due to the state error at the beginning.

Like in the delivery mission, the Coulomb-counting method does not provide the desired results for the reasons explained in the previous section. Both Kalman filters can quickly correct the errors and closely match the change in SOC. The maximum error and RMSE of the estimation methods are listed in Table 6.

The maximum deviation is the same range as the maximum deviation of the first flight mission because it is caused by the initial conditions. Comparing the RMSE values of both Kalman filters, the unscented Kalman filter (0.24%) is more accurate than the extended Kalman filter (1.58%) as expected. The deviation profiles of both Kalman filters during the mission in Figure 17 show this as well. Both Kalman filters correct the SOC error quickly, but the extended Kalman filter has trouble eliminating the error completely. The performance of the unscented Kalman filter is about 84.81% more accurate than the extended Kalman filter.

The estimation of the facade inspection mission is more accurate than the estimation of the delivery mission, as all estimators have a more accurate performance than the estimators for the delivery mission. Due to the different load requirements, the current and thus the behavior of the model change. Thus, the load changes result in different performance of the state estimators. Despite the differences in performance due to the power profile, the best fitting estimator is the unscented Kalman filter as expected.

To compare the deviations of the estimated SOC and the real SOC for both missions, the absolute deviations of the best performing filter, the unscented Kalman filter, are plotted against the SOC in Figure 18. The estimation error of 4% at the beginning of the missions due to the different starting conditions are trimmed to make the deviations

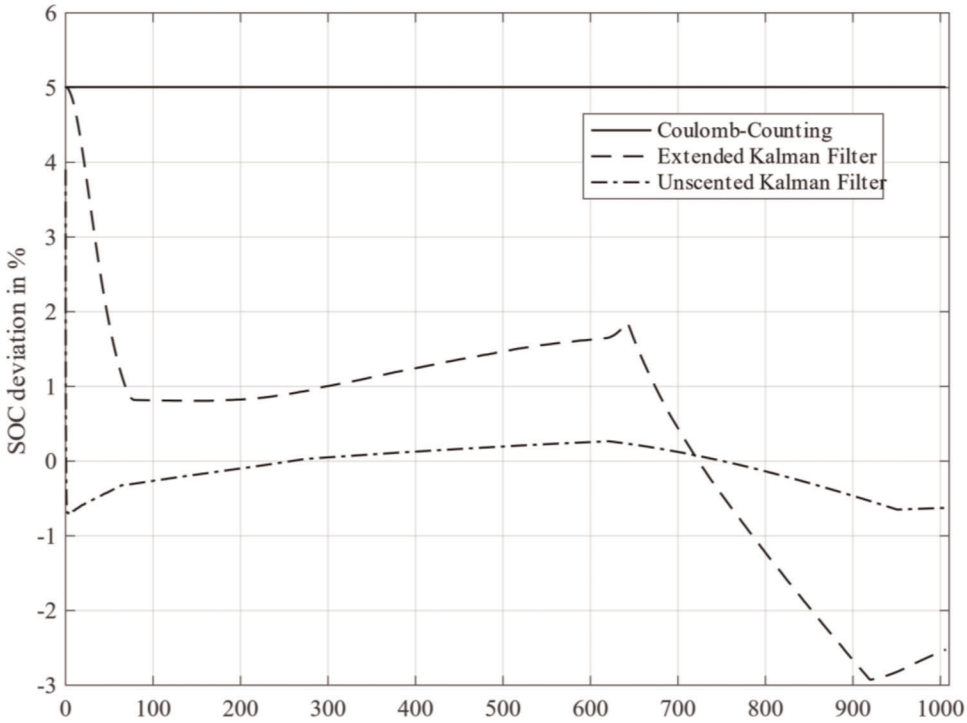

Figure 14. Deviation of the estimation methods from the real SOC for the delivery flight mission.

Table 4
Maximum deviation and RMSE of the estimation methods in comparison to the UAV battery SOC.

	Maximum deviation (%)	**RMSE (%)**
Coulomb-counting	5.02	4.99
Extended Kalman filter	5.01	1.76
Unscented Kalman filter	3.02	0.30

during the mission more visible. It can be seen that the deviation depends more on the SOC value than on the load and the corresponding current for the investigated battery and flight mission. This proves that parameter identification is one of the most important processes for estimating SOC reliability. If the battery parameter estimation differs from the real battery parameter, the SOC estimation will not be as reliable, as can be seen here. For parameters that are extremely different from those of the real system, the Kalman filters will not converge to the system and the estimates will fail. A solution approach to avoid this divergence problem is a parameter estimation within a SOC estimation as in Yang et al. (2019) or Mondal et al. (2022).

In summary, estimation with the unscented Kalman filter provides more accurate results for estimating the SOC compared to the extended Kalman filter, as expected. The performance of the unscented Kalman filter across both missions is within an RMS error of 0.3% while the extended Kalman filter performance is within an error of 1.7%. However, both filter techniques are significantly better than using simple Coulomb-counting. The extended Kalman filter is not as accurate as the unscented Kalman filter but can still be used for dynamic processes. The most important impact on the estimation method is the accuracy of the parameter identification.

Further focal points to justify the choice of a Kalman filter would be the consideration against strongly differing initial conditions or stronger measurement noise, also called robustness. To estimate the time correctly and to make the estimation more reliable, an implementation of an adaptive unscented Kalman filter as in Fu et al. (2022) and Zheng et al. (2018) would be a solution approach. Another approach is to use a particle filter as in Tang et al. (2020) or Luan et al. (2023).

3.2 Estimation of EOD

To estimate the remaining flight time of the UAV during a mission, the influence of the SOC estimation methods on the discharge time estimation is also evaluated. To evaluate the estimation of the EOD, the results are compared to the value of a constant current discharge for each mission calculated in Section 3.1 as a reference.

For the delivery flight mission, the EOD is about 1028.2 s at an assumed constant discharge rate of −0.07%/s This is only about 22 s after the end of the mission. However, it should be noted that this paper considers the lower end of the operation range of the battery as the EOD and not the point of 0% SOC.

Table 7 shows the results of estimating the time of discharge with the three different SOC estimation methods.

Table 5
Comparison of the end of mission SOC values of the battery and the respective estimation method for the facade mission.

Battery	Unscented Kalman filter	Extended Kalman filter	Coulomb-Counting
54.06%	54.29%	55.79%	59.06%

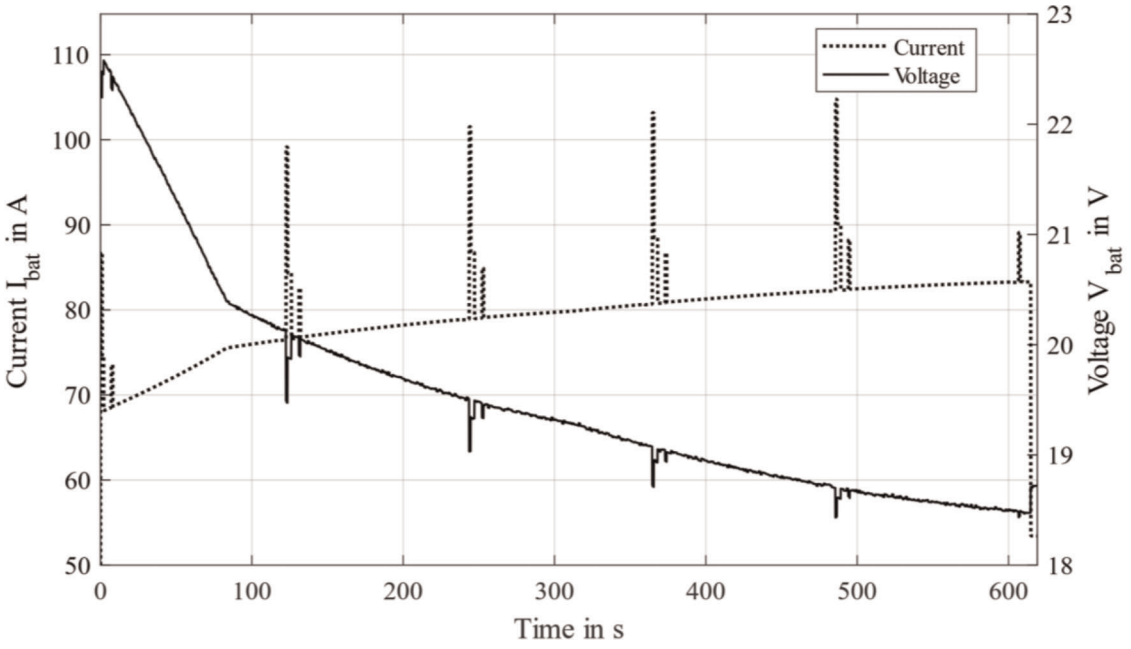

Figure 15. Resulting current and voltage profiles of the UAV battery during the facade inspection mission.

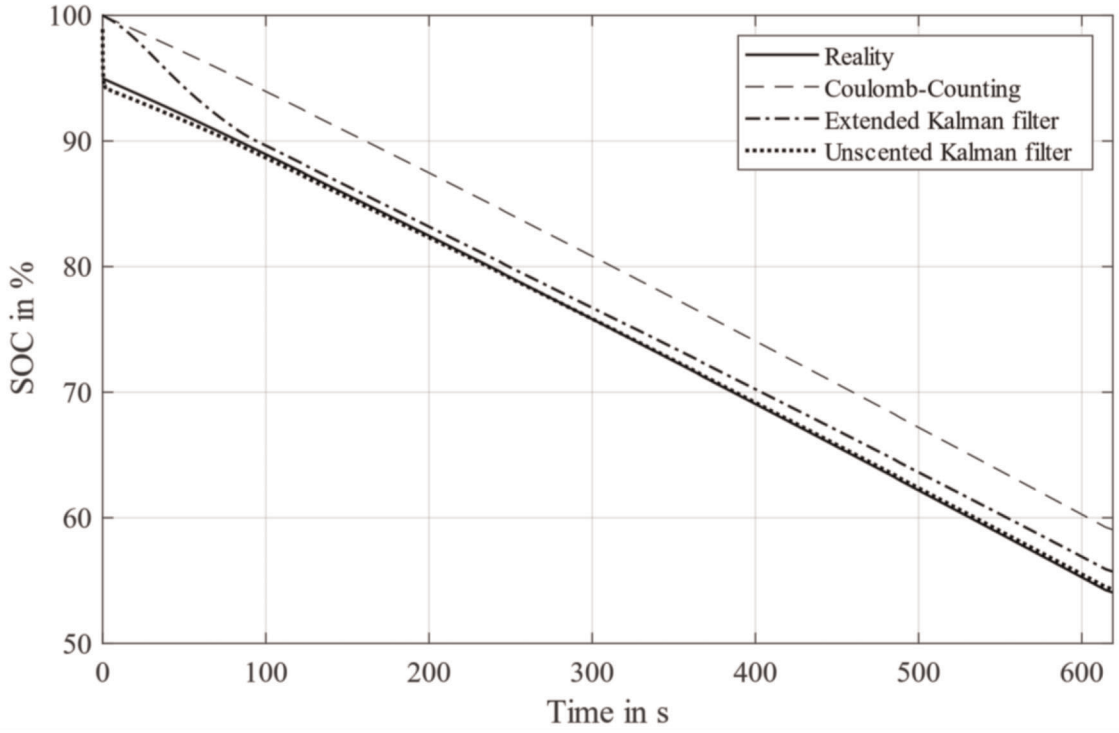

Figure 16. Resulting SOC profiles of the UAV battery and the estimation methods during the facade inspection mission.

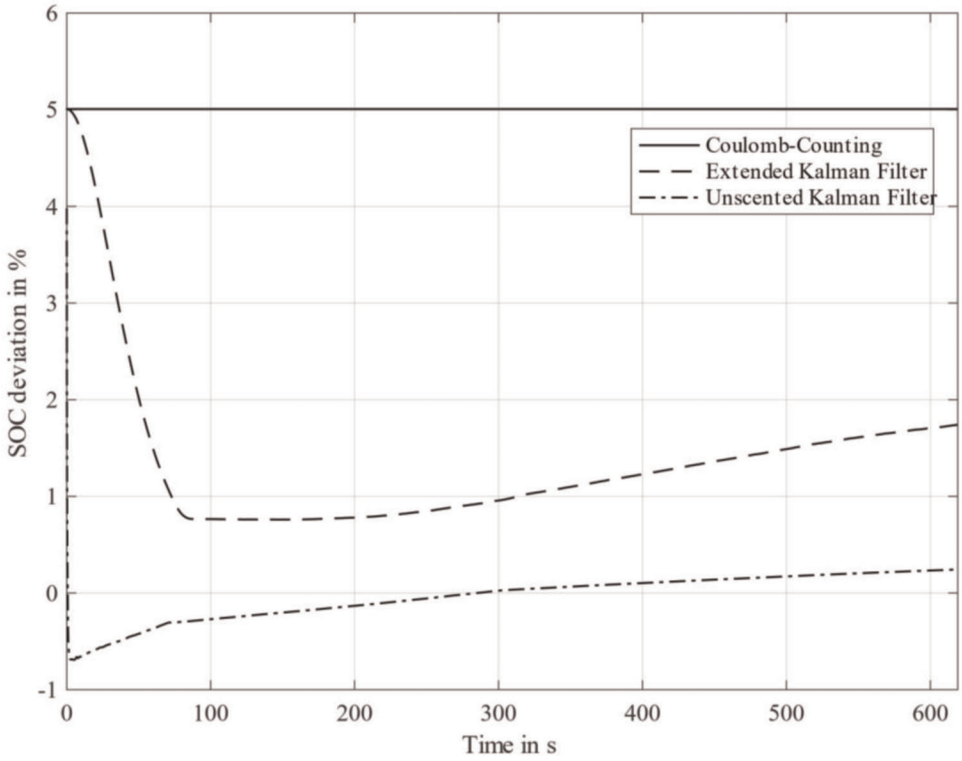

Figure 17. SOC deviation profiles for the facade inspection mission from the considered estimation methods.

Table 6
Maximum error and RMSE of the estimation methods in comparison to the UAV battery SOC.

	Maximum deviation (%)	**RMSE (%)**
Coulomb-counting	5.10	5.01
Extended Kalman filter	5.01	1.58
Unscented Kalman filter	3.91	0.24

The deviation of the estimation from the reference time is shown in the third column of the table.

The results of the Coulomb-counting method have the highest deviation between the calculated and the estimated EOD with 15.13% compared to the extended and the unscented Kalman filters. Due to the different initial conditions and the failed SOC estimation, the EOD estimation is not as accurate as desired. The estimated EOD points of the extended and unscented Kalman filters fit well, as the deviation between the calculated and estimated EOD points is less than 1%. However, the unscented Kalman filter outperforms the extended Kalman filter.

For the facade inspection mission, the EOD with a constant current draw of 79.24 A (average current of the mission) is calculated at 1133.8 s. The EOD estimates (shown in Table 8) of all methods deviate strongly from the reference mean by 18.24% to 23.69%. A possible reason could be the strong current decrease at the end of the mission due to the landing maneuver (see Figure 15). Therefore, the methods estimated a later discharge end point. The observed time interval for the estimated discharge point is too small. To validate the EOD estimate in the facade inspection mission, the EOD estimate is taken at 614.6 s without the landing maneuver.

The improved results are shown in Table 9. The new calculated deviations are smaller than before with a deviation of the Kalman filters of about 1%, so the Kalman filter EOD estimation works well for the facade inspection mission. The unscented Kalman filter again outperforms the extended Kalman filter.

Furthermore, it is noticeable that the EOD estimation for the facade inspection mission does not achieve better results like in the SOC estimation. So, the deviation of the Kalman filter is not necessarily related to the accuracy of the EOD estimation. The EOD estimation is more dependent on the dynamic load than the SOC estimation.

Overall, the estimation of the EOD is very sensitive to small changes in the current at the end of a flight mission. To improve the estimation and change the robustness, the moving average factor could be changed to increase the observed interval. The combination of the SOC estimator with a subsequent EOD estimator represents a sensitive system that is difficult to tune to implement uniformity across many different UAV flight missions. It may be more reliable to combine the adaptive unscented Kalman filter with a neural network if sufficient training data are generated to improve the SOC and EOD estimations, as in Hannan et al. (2017) and Cui et al. (2022).

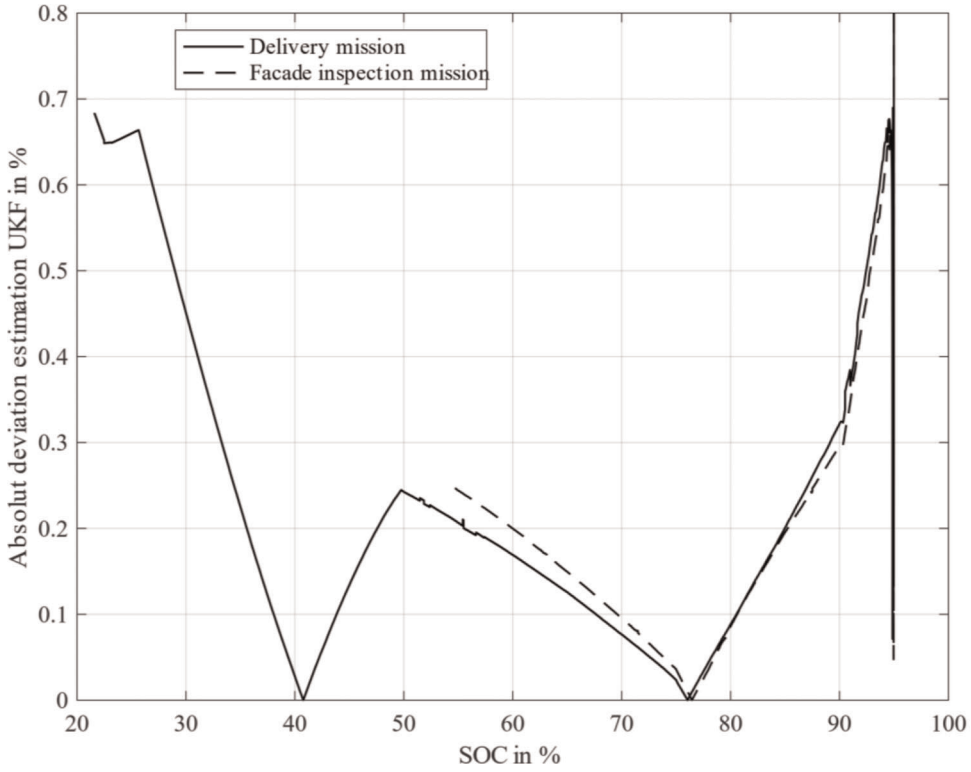

Figure 18. Absolute SOC deviation as a function of SOC value for both missions.

Table 7
Results of EOD estimation for the delivery flight mission and the deviation from the reference constant current EOD.

	EOD (s)	Deviation (%)
Coulomb-counting	1183.8	15.13
Extended Kalman filter	1036.7	0.82
Unscented Kalman filter	1030.1	0.18

Table 8
Results of EOD estimate for the facade inspection mission and the deviation from the reference constant current EOD.

	EOD (s)	Deviation (%)
Coulomb-counting	1485.9	23.69
Extended Kalman filter	1442.7	21.41
Unscented Kalman filter	1386.7	18.24

Table 9
Corrected results of EOD estimation for the facade inspection mission and the deviation from the reference constant current EOD.

	EOD (s)	Deviation (%)
Coulomb-counting	1179.1	3.84
Extended Kalman filter	1115.1	1.68
Unscented Kalman filter	1145.4	1.01

4 Conclusion and Outlook

In this paper, a multirotor UAV battery model has been developed and different Kalman filters and the Coulomb-counting method have been compared with respect to their performance in estimating the load-dependent SOC and EOD of the UAV battery. A 2RC-equivalent circuit battery model is used in combination with different estimation methods. The varying loads of two power profiles of UAV flight missions were simulated using the Coulomb-counting method, the extended Kalman filter, and the unscented Kalman filter. In addition, the EOD estimation was tested with the estimated states.

In conclusion, the SOC of the analyzed UAV and the different flight missions can be estimated with both an unscented Kalman filter and an extended Kalman filter. Only the Coulomb-counting method does not achieve good results. The unscented Kalman filter achieves more accurate results due to the nonlinearity of the system, as expected and in line with the existing literature.

The deviation between the delivery and the facade inspection missions for the estimation by the unscented Kalman filter is slightly different. Comparing the deviations as a function of the SOC, it is clear that the deviations depend mostly on the SOC and less on the variation of the load and the corresponding current. The main cause of the deviations is the parameter identification and its deviation between reality and model. Therefore, parameter identification and the evaluation of the model with a real system play an important role in the development of a digital twin.

The estimation of the EOD works reliably for the delivery mission as well as for the facade inspection mission. The deviations depend more on the dynamic load of the mission. Therefore, the facade inspection mission leads to less accurate EOD estimations. Nevertheless, the unscented Kalman filter in combination with the EOD estimation achieves more accuracy. Overall, the system is sensitive and a small change in the Kalman filter tuning could have a large impact on the EOD estimation.

To correctly estimate the SOC during the mission, an appropriate estimation method must be chosen. The method also depends on the parameters. If the parameters have high nonlinearity and linearization around the operation point is difficult, an extended Kalman filter or an unscented Kalman filter will archive less accurate results in SOC and EOD estimation compared to systems with low nonlinearity. To improve SOC estimation, the estimation method of choice should be adaptive. There are several different estimation techniques that could be tested, such as the adaptive unscented Kalman filter with correntropy loss in Sun et al. (2018) or the estimation with a long short-term memory network as in Gong et al. (2022), or resorting to a neural network and a training set that collects data during missions and can use this information for a better estimation.

Reliable parameter identification is essential for the choice of the SOC estimator. Since parameter identification often leads to deviation and the parameters could change due to degradation effect, a combination of parameter and SOC estimation could be a solution approach as in Mondal et al. (2022).

The two studied flight mission examples show that the estimation of SOC can also be applied to UAV batteries. The filters achieve results comparable to those of existing literature, which indicates a lower impact of the dynamic load requirements of a UAV mission on the choice of the estimation method.

For further work and to explore the application of SOC estimation more deeply, the influences of other environmental aspects would need to be considered. Also, the robustness of the extended Kalman filter and the unscented Kalman filter should be analyzed and a combination with a neural network should be tested. In combination with a state-of-health estimation, the system would become more sensitive, so the SOC estimation should work as reliably as possible.

A robust SOC estimation is required with a more advanced battery model of a digital twin, as there are additional aspects to consider, such as degradation of the battery. The degradation could be estimated with a state-of-health estimation process as in Noura et al. (2020) or a battery lifetime prediction could be implemented as in Yang et al. (2022). Furthermore, the effect of temperature on the UAV parameters needs to be analyzed as in Yang et al. (2019).

In addition, experimental validation of the battery model by measuring real-time data of a UAV battery and implementation of a microcontroller for communication are planned for future work.

References

Anggraeni, D., Sudiarto, B., Subhan, A., Chasanah, N., Santosa, C. E., Suryanti, D. I., Prabowo, G. S., & Priambodo, P. S. (2022). SOC estimation lithium polymer battery based on equivalent circuit model and extended Kalman filter. *2022 5th Asia Conference on Energy and Electrical Engineering (ACEEE)*. https://doi.org/10.1109/aceee56193.2022.9851867

Ayamga, M., Akaba, S., & Nyaaba, A. A. (2021). Multifaceted applicability of drones: A review. *Technological Forecasting and Social Change*, *167*, 120677. https://doi.org/10.1016/j.techfore.2021.120677

Boulmrharj, S., Ouladsine, R., NaitMalek, Y., Bakhouya, M., Zine-dine, K., Khaidar, M., & Siniti, M. (2020). Online battery state-of-charge estimation methods in micro-grid systems. *Journal of Energy Storage*, *30*, 101518. https://doi.org/10.1016/j.est.2020.101518

Boulos, M. N. K., & Zhang, P. (2021). Digital twins: From personalised medicine to precision public health. *Journal of Personalized Medicine*, *11*(8), 745. https://doi.org/10.3390/jpm11080745

Cui, Z., Dai, J., Sun, J., Li, D., Wang, L., & Wang, K. (2022). Hybrid methods using neural network and Kalman filter for the state of charge estimation of lithium-ion battery. *Mathematical Problems in Engineering*, *2022*, 9616124. https://doi.org/10.1155/2022/9616124

Fakhraian, E., Semanjski, I., Semanjski, S., & Aghezzaf, E.-H. (2023). Towards safe and efficient unmanned aircraft system operations: Literature review of digital twins' applications and European Union regulatory compliance. *Drones*, *7*(7), 478. https://doi.org/10.3390/drones7070478

Fu, Y., Zhai, B., Shi, Z., Liang, J., & Peng, Z. (2022). State of charge estimation of lithium-ion batteries based on an adaptive iterative extended Kalman filter for AUVs. *Sensors*, *22*(23), 9277. https://doi.org/10.3390/s22239277

Gong, L., Zhang, Z., Li, Y., Li, X., Sun, K., & Tan, P. (2022). Voltage-stress-based state of charge estimation of pouch lithium-ion batteries using a long short-term memory network. *Journal of Energy Storage*, *55*, 105720. https://doi.org/10.1016/j.est.2022.105720

Guo, J., Liu, S., & Zhu, R. (2023). An unscented Kalman filtering method for estimation of state-of-charge of lithium-ion battery. *Frontiers in Energy Research*, *10*, 998002. https://doi.org/10.3389/fenrg.2022.998002

Hannan, M. A., Lipu, M. S. H., Hussain, A., & Mohamed, A. (2017). A review of lithium-ion battery state of charge estimation and management system in electric vehicle applications: Challenges and recommendations. *Renewable and Sustainable Energy Reviews*, *78*, 834–854. https://doi.org/10.1016/j.rser.2017.05.001

Hassani, H., Huang, X., & MacFeely, S. (2022). Impactful digital twin in the healthcare revolution. *Big Data and Cognitive Computing*, *6*(3), 83. https://doi.org/10.3390/bdcc6030083

He, H., Qin, H., Sun, X., & Shui, Y. (2013). Comparison study on the battery SoC estimation with EKF and UKF algorithms. *Energies*, *6*(10), 5088–5100. https://doi.org/10.3390/en6105088

Hu, X., Sun, F., & Zou, Y. (2010). Estimation of state of charge of a lithium-ion battery pack for electric vehicles using an adaptive Luenberger observer. *Energies*, *3*(9), 1586–1603. https://doi.org/10.3390/en3091586

Hu, Z., Ren, G., Zhang, J., Si, Y., & Duan, Y. (2023). A parameter identification and state of charge estimation method of lithium-ion battery considering temperature bias. *Journal of Energy Storage*, *68*, 107650. https://doi.org/10.1016/j.est.2023.107650

Huang, C., Wang, Z., Zhao, Z., Wang, L., Lai, C. S., & Wang, D. (2018). Robustness evaluation of extended and unscented Kalman filter for battery state of charge estimation. *IEEE Access*, *6*, 27617–27628. https://doi.org/10.1109/access.2018.2833858

Huria, T., Ceraolo, M., Gazzarri, J., & Jackey, R. (2012). High fidelity electrical model with thermal dependence for characterization and simulation of high power lithium battery cells. *2012 IEEE International Electric Vehicle Conference*. https://doi.org/10.1109/ievc.2012.6183271

Huria, T., Ceraolo, M., Gazzarri, J., & Jackey, R. (2013). Simplified extended Kalman filter observer for SOC estimation of commercial power-oriented LFP lithium battery cells. *SAE Technical Paper Series*, 2013-01-1544. https://doi.org/10.4271/2013-01-1544

Jackey, R. A., Saginaw, M., Sanghvi, P., Gazzarri, J., Huria, T., & Ceraolo, M. (2013). Battery model parameter estimation using a layered technique: an example using a lithium iron phosphate cell. *SAE Technical Paper Series*. https://doi.org/10.4271/2013-01-1547

Jung, S., & Jeong, H. (2017). Extended Kalman filter-based state of charge and state of power estimation algorithm for unmanned aerial vehicle Li-Po battery packs. *Energies*, *10*(8), 1237. https://doi.org/10.3390/en10081237

Khanum, F., Louback, E., Duperly, F., Jenkins, C., Kollmeyer, P. J., & Emadi, A. (2021). A Kalman filter based battery state of charge estimation MATLAB function. *2021 IEEE Transportation Electrification Conference & Expo (ITEC)* (pp. 484–489). https://doi.org/10.1109/itec51675.2021.9490163

Khawaja, Y., Shankar, N. G., Qiqieh, I., Alzubi, J. A., Alzubi, O. A., Nallakaruppan, M., & Padmanaban, S. (2023). Battery management solutions for Li-ion batteries based on artificial intelligence. *Ain Shams Engineering Journal*, 102213. https://doi.org/10.1016/j.asej.2023.102213

Klima New York City—wetter.de. (n.d.). Retrieved from https://www.wetter.de/klima/nordamerika-mittelamerika/usa/new-york-city-s99000050.html

Krupp, A., Beckmann, R., Diekmann, T., Ferg, E., Schuldt, F., & Agert, C. (2022). Calendar aging model for lithium-ion batteries considering the influence of cell characterization. *Journal of Energy Storage*, *45*, 103506. https://doi.org/10.1016/j.est.2021.103506

Kumar, S., & Rao, S. K. (2023). State of charge estimation of Li-ion battery using unscented Kalman filter. *BioGecko Journal for New Zealand Herpetology*, *12*(02). https://biogecko.co.nz/admin/uploads/Updated%20Manuscript%20(2).pdf

Lanteigne, A., Kibru, E., Azam, S., & Al Shammary, S. (2017). Design of a drone lead-follow control system. *2017 Systems and Information Engineering Design Symposium (SIEDS)* (pp. 162–167). https://doi.org/10.1109/sieds.2017.7937709

Lithium Battery Cell—MathWorks Deutschland. (n.d.). Retrieved from https://de.mathworks.com/help/simscape/ug/lithium-battery-cell-two-rc-branch-equivalent-circuit.html

Liu, S., Dong, X., Yu, X., Ren, X., Zhang, J., & Zhu, R. (2022). A method for state of charge and state of health estimation of lithium-ion battery based on adaptive unscented Kalman filter. *Energy Reports*, *8*, 426–436. https://doi.org/10.1016/j.egyr.2022.09.093

Luan, Z., Qin, Y., Hu, B., Zhao, W., & Wang, C. (2023). Estimation of state of charge for hybrid unmanned aerial vehicle Li-ion power battery for considering rapid temperature change. *Journal of Energy Storage*, *59*, 106479. https://doi.org/10.1016/j.est.2022.106479

Lv, J., Jiang, B., Wang, X., Liu, Y., & Fu, Y. (2020). Estimation of the state of charge of lithium batteries based on adaptive unscented Kalman filter algorithm. *Electronics*, *9*(9), 1425. https://doi.org/10.3390/electronics9091425.

Madni, A. M., Madni, C. C., & Lucero, S. D. (2019). Leveraging digital twin technology in model-based systems engineering. *Systems*, *7*(1), 7. https://doi.org/10.3390/systems7010007

Manoharan, A., Sooriamoorthy, D., Begam, K. M., & Aparow, V. R. (2023). Electric vehicle battery pack state of charge estimation using parallel artificial neural networks. *Journal of Energy Storage*, *72*, 108333. https://doi.org/10.1016/j.est.2023.108333

Matrice 600 Pro—DJI. (n.d.). Retrieved from https://www.dji.com/de/matrice600-pro/info#specs

Meng, J., Luo, G., Ricco, M., Swierczynski, M., Stroe, D.-I., & Teodorescu, R. (2018). Overview of lithium-ion battery modeling methods for state-of-charge estimation in electrical vehicles. *Applied Sciences*, *8*(5), 659. https://doi.org/10.3390/app8050659

Mondal, A., Routray, A., & Puravankara, S. (2022). Parameter identification and co-estimation of state-of-charge of Li-ion battery in real-time on Internet-of-Things platform. *Journal of Energy Storage*, *51*, 104370. https://doi.org/10.1016/j.est.2022.104370

Naseri, F., Gil, S., Barbu, C., Cetkin, E., Yarimca, G., Jensen, A. C., Larsen, P. G., & Gomes, C. (2023). Digital twin of electric vehicle battery systems: Comprehensive review of the use cases, requirements, and platforms. *Renewable & Sustainable Energy Reviews*, *179*, 113280. https://doi.org/10.1016/j.rser.2023.113280

Nasirahmadi, A., & Hensel, O. (2022). Toward the next generation of digitalization in agriculture based on digital twin paradigm. *Sensors*, *22*(2), 498. https://doi.org/10.3390/s22020498

Noura, N., Boulon, L., & Jemeï, S. (2020). A review of battery state of health estimation methods: Hybrid electric vehicle challenges. *World Electric Vehicle Journal*, *11*(4), 66. https://doi.org/10.3390/wevj11040066.

Possoch, M., Bieker, S., Hoffmeister, D., Bolten, A., Schellberg, J., & Bareth, G. (2016). Multi-temporal crop surface models combined with the RGB vegetation index from UAV-based images for forage monitoring in grassland. *ISPRS—International Archives of the Photogrammetry, Remote Sensing and Spatial Information Sciences*, *XLI-B1*, 991–998. https://doi.org/10.5194/isprsarchives-xli-b1-991-2016

Priya, R. P., Sanjay, R., & Sakile, R. (2022). State of charge estimation of lithium-ion battery based on extended Kalman filter and unscented Kalman filter techniques. *Energy Storage*, *5*(3), e408. https://doi.org/10.1002/est2.408

Raoofi, T., & Yildiz, M. (2023). Comprehensive review of battery state estimation strategies using machine learning for battery management systems of aircraft propulsion batteries. *Journal of Energy Storage*, *59*, 106486. https://doi.org/10.1016/j.est.2022.106486

Saji, D., Babu, P. S., & Ilango, K. (2019). SoC estimation of lithium ion battery using combined coulomb counting and fuzzy logic method, *2019 4th International Conference on Recent Trends on Electronics, Information, Communication & Technology (RTEICT)* (pp. 948–952). https://doi.org/10.1109/rteict46194.2019.9016956

Sangwan, V., Kumar, R., & Kumar Rathore, A. (2019). State-of-charge estimation of Li-ion battery at different temperatures using particle filter. *Journal of Engineering*, *2019*(18), 5320–5324. https://doi.org/10.1049/joe.2018.9234

Santos, R. M., Alves, C. L., Macedo, E. C., Villanueva, J. M., & Hartmann, L. V. (2017). Estimation of lithium-ion battery model parameters using experimental data. *2017 2nd International Symposium on Instrumentation Systems, Circuits and Transducers (INSCIT)* (pp. 1–6). https://doi.org/10.1109/inscit.2017.8103527

Schacht-Rodriguez, R., Ortiz-Torres, G., Garcia-Beltra, C. D., Astorga-Zaragoza, C. M., Ponsart, J. C., & Theilliol, D. (2017). SoC estimation using an extended Kalman filter for UAV applications. *2017 International Conference on Unmanned Aircraft Systems (ICUAS)* (pp. 179–187). https://doi.org/10.1109/icuas.2017.7991381

Sepasi, S., Ghorbani, R., & Liaw, B. Y. (2014). A novel on-board state of charge estimation method for aged Li-ion batteries based on model adaptive extended Kalman filter. *Journal of Power Sources*, *245*, 337–344. https://doi.org/10.1016/j.powsour.2013.06.108

Shibl, M. M., Ismail, L. S., & Massoud, A. M. (2023). A machine learning-based battery management system for state-of-charge prediction and state-of-health estimation for unmanned aerial vehicles.

Journal of Energy Storage, *66*, 107380. https://doi.org/10.1016/j.est.2023.107380

Shrivastava, P., Soon, T. K., Idris, M. Y., & Mekhilef, S. (2019). Overview of model-based online state-of-charge estimation using Kalman filter family for lithium-ion batteries. *Renewable and Sustainable Energy Reviews*, *113*, 109233. https://doi.org/10.1016/j.rser.2019.06.040

Singh, S., Weeber, M., & Birke, K. P. (2021). Implementation of battery digital twin: Approach, functionalities and benefits. *Batteries*, *7*(4), 78. https://doi.org/10.3390/batteries7040078

Soliman, A., Al-Ali, A., Mohamed, A., Gedawy, H., Izham, D., Bahri, M., & Guizani, M. (2023). AI-based UAV navigation framework with digital twin technology for mobile target visitation. *Engineering Applications of Artificial Intelligence*, *123*, 106318. https://doi.org/10.1016/j.engappai.2023.106318

Sun, Q., Zhang, H., Zhang, J., & Ma, W. (2018). Adaptive unscented Kalman filter with correntropy loss for robust state of charge estimation of lithium-ion battery. *Energies*, *11*(11), 3123. https://doi.org/10.3390/en11113123

Sun, Y., Fesenko, H., Kharchenko, V., Zhong, L., Kliushnikov, I., Illiashenko, O., Morozova, O., & Sachenko, A. (2022). UAV and IoT-based systems for the monitoring of industrial facilities using digital twins: Methodology, reliability models, and application. *Sensors*, *22*(17), 6444. https://doi.org/10.3390/s22176444

Suwe, M., de Groot, A., Forner, M., & Werner, C. (2022). Model-based development of multirotor UAV power profiles for performance investigation of different flight missions. *Journal of Aviation Technology and Engineering*, *11*(1), 19–36. https://doi.org/10.7771/2159-6670.1245

Tang, D. Y., Gong, M. T., Yu, J. S., & Li, X. (2020). A power transfer model-based method for lithium-ion battery discharge time prediction of electric rotatory-wing UAV. *Microelectronics Reliability*, *114*, 113832. https://doi.org/10.1016/j.microrel.2020.113832

Thelen, A., Zhang, X., Fink, O., Lu, Y., Ghosh, S., Youn, B. D., Todd, M. D., Mahadevan, S., Hu, C., & Hu, Z. (2022). A comprehensive review of digital twin—Part 2: Roles of uncertainty quantification and optimization, a battery digital twin, and perspectives. *Structural and Multidisciplinary Optimization*, *66*(1), Article 1. https://doi.org/10.1007/s00158-022-03410-x

Yang, D., Cui, Y., Xia, Q., Jiang, F., Ren, Y., Sun, B., Feng, Q., Wang, Z., & Yang, C. (2022). A digital twin-driven life prediction method of lithium-ion batteries based on adaptive model evolution. *Materials*, *15*(9), 3331. https://doi.org/10.3390/ma15093331

Yang, Y., Dong, A., Li, Y., Ahmed, R., & Emadi, A. (2019). Temperature dependent state of charge estimation of lithium-ion batteries using long short-term memory network and Kalman filter. *IECON 2019, 45th Annual Conference of the IEEE Industrial Electronics Society* (pp. 4335–4340). https://doi.org/10.1109/iecon.2019.8927710

Ye, M., Guo, H., Xiong, R., & Yu, Q. (2018). A double scale and adaptive particle filter-based online parameter and state of charge estimation method for lithium-ion batteries. *Energy*, *114*, 789–799. https://doi.org/10.1016/j.energie.2017.12.061

Zhang, H., Zhou, M., & Lan, X. (2019). State of charge estimation algorithm for unmanned aerial vehicle power-type lithium battery packs based on the extended Kalman filter. *Energies*, *12*(20), 3960. https://doi.org/10.3390/en12203960

Zhang, S., Zhang, C., Jiang, S., & Zhang, X. (2022). A comparative study of different adaptive extended/unscented Kalman filters for lithium-ion battery state-of-charge estimation. *Energy*, *246*, 123423. https://doi.org/10.1016/j.energy.2022.123423

Zhao, P., Li, M., Kang, J., & Rizzoni, G. (2017). Analysis of fading characteristics of a lithium ion battery based on an integration model. *International Journal of Heat and Mass Transfer*, *104*, 1317–1324. https://doi.org/10.1016/j.ijheatmasstransfer.2016.09.083

Zheng, B., Fu, P., Li, B., & Yuan, X. (2018). A robust adaptive unscented Kalman filter for nonlinear estimation with uncertain noise covariance. *Sensors*, *18*(3), 808. https://doi.org/10.3390/s18030808

Zhou, W., Zheng, Y., Pan, Z., & Lu, Q. (2021). Review on the battery model and SOC estimation method. *Processes*, *9*(9), 1685. https://doi.org/10.3390/pr9091685

Zhu, C., Li, X., Song, L., & Xiang, L. (2013). Development of a theoretically based thermal model for lithium ion battery pack. *Journal of Power Sources*, *223*, 155–164. https://doi.org/10.1016/j.jpowsour.2012.09.035